Determination of Area fraction of Free Lime in Steelmaking Slag Using Cathodoluminescence and X-ray Excited Optical Luminescence

doi: 10.1007/s11663-020-01927-4

Metall. Mater. Trans. B, 51B (2020) 2003-2011.
[DOI: 10.1007/s11663-020-01927-4]

Determination of Area fraction of Free Lime in Steelmaking Slag Using Cathodoluminescence and X-ray Excited Optical Luminescence

Susumu Imashuku[*1] and Kazuaki Wagatsuma[*1]

[*1] Institute for Materials Research, Tohoku University

Abstract

Determining the free lime (f-CaO) content in steelmaking slag is critical for road construction because f-CaO is likely to cause road expansion. Herein, we present a method to determine an area fraction of f-CaO from fractions of illuminated areas related to f-CaO in cathodoluminescence (CL) and X-ray excited optical luminescence (XEOL) images of industrial steelmaking slag, which is simpler and quicker than the commonly employed ethylene glycol extraction method. A heat-treatment that was quenched the industrial steelmaking slag from 1000 °C was needed to obtain intense luminescence from f-CaO, which originated from a peak at 600 nm. Other mineral phases, such as Ca_2SiO_4, free magnesia, and $2CaO{\cdot}Al_2O_3{\cdot}SiO_2$, were distinguishable from f-CaO from their luminescent colors. When we analyzed three types of industrial steelmaking slag with different f-CaO contents, the order of the fractions of the illuminated areas originating from f-CaO in the CL images was consistent with that of the f-CaO content measured applying the ethylene glycol extraction method. The average exposure times it took the CL and XEOL images to detect the luminescence from f-CaO were 5 and 30 s, respectively. In particular, acquiring XEOL images is promising for on-site analysis

Keywords : Steel slag, Quantitative-determination, Rapid identification

1. INTRODUCTION

In the steelmaking process, huge amounts of steelmaking slag, which is a byproduct of the conversion of carbon-rich molten iron to steel in basic oxygen furnaces (BOFs) and the conversion of scrap to steel electric arc furnaces (EAFs), are produced globally. Recently, the reuse of steelmaking slag has been aggressively tackled in the iron and steelmaking industry to realize an environmentally friendly society. The reuse rate of steelmaking slag is close to 100% in developed countries such as the United States, Japan, Germany, and France.[1-2] In these countries, almost half of the reused steelmaking slag is used in road construction, e.g., road bases, embankments, and asphaltic concrete.[1-6] Steelmaking slag contains free lime (f-CaO), which can cause volumetric expansion because it doubles in volume upon reacting with the water and carbon dioxide in the air.[7-8] Therefore, prior to its use in road construction, steelmaking slag is aged, i.e., exposed to air, sprayed with hot water, or steamed,[9] to accelerate the hydration and carbonation reactions of f-CaO. Various aging periods have been proposed, e.g., 1–18 months for exposure periods in air because the required aging period depends on the amount of f-CaO in the steelmaking slag.[6] If the aging is insufficient, the residual f-CaO is likely to create serious problems, such as road expansion and cracking.[6] As such, determining the f-CaO content in steelmaking slag before and after aging is crucial to efficiently and safely use steelmaking slag for road construction.

Several methods to determine the f-CaO content in steelmaking slag have been proposed, such as ethylene glycol extraction followed by the determination of calcium in the ethylene glycol *via* titration, atomic absorption spectrophotometry, or inductively coupled plasma-atomic emission spectrometry (ICP-AES),[9-11] X-ray diffraction (XRD),[12-15] and infrared spectrophotometry.[16] Among these methods, the ethylene glycol extraction method is the most commonly used. However, the f-CaO content determined applying this method also includes the $Ca(OH)_2$ content in the steelmaking slag because both are extracted in the ethylene glycol.[15,17] To obtain an accurate f-CaO measure, a combined method of the ethylene glycol extraction and thermogravimetry, which can also determine the $Ca(OH)_2$ content in steelmaking slag, has been proposed.[18] Extraction *via* ethylene glycol is a complicated and time-consuming procedure requiring skillful techniques, e.g., controlling the particle size of the steelmaking slag and monitoring the temperature and extraction time.[18] Therefore, a simple method to rapidly determine the f-CaO content in steelmaking slag would

contribute to the reduction of the time needed to analyze and master the techniques.

We have recently demonstrated that cathodoluminescence (CL) analysis can rapidly and simply identify f-CaO in steelmaking slag samples synthesized from reagents.[19] A CL analysis involves obtaining images and spectra based on the phenomenon of light emission by electron bombardment. In this method, f-CaO emits intense orange luminescence related to manganese (II) ions (Mn^{2+}), which are dissolved into the f-CaO, in the CL images of the synthesized steelmaking slag samples, whereas the other mineral phases, e.g., $3CaO{\cdot}SiO_2$, $2CaO{\cdot}SiO_2$, $2CaO{\cdot}Fe_2O_3$, and wüstite (FeO dissolving MnO), do not exhibit such intense luminescence. Based on these results, we have considered that f-CaO in industrial steelmaking slag can be quantitatively analyzed by evaluating its related illuminated areas in CL images. The purpose of this study is to suggest a novel practical CL imaging method to rapidly determine the area fraction of f-CaO in industrial steelmaking slag. To establish this method, we obtain and investigate the CL images and spectra of several mineral phases in industrial steelmaking slag samples to distinguish f-CaO from other minerals. Following this, we use X-ray excited optical luminescence (XEOL), which is used to obtain images and spectra based on the phenomenon of light emission by X-ray irradiation, for its application to on-site determination of the area fraction of f-CaO in steelmaking slag because XEOL can be performed in the air.

2. EXPERIMENTAL

A CL analysis was conducted for industrial BOF and EAF slag samples by-produced in practical operations in Nippon Steel Corp. and JFE Steel Corp; none of the samples had been aged. The basicity (CaO/SiO_2 ratio) and f-CaO content of the industrial slag samples are listed in Table I. Concentrations of other components, such as CaO, SiO_2, Al_2O_3, MgO, MnO, P_2O_5, S, and total Fe, in the slag samples were similar to those of typical BOF and EAF slags.[9,20] To determine the component concentrations for each slag sample *via* ICP-AES, dozens of slag lumps whose total weight were approximately 50 g were crushed together into powders and tens of grams of the powders were used for the determination. Each batch of the industrial slag samples (slags A, B, and C) for CL measurement consisted of several pieces of slag weighting approximately 5 g. Prior to the CL measurement, the surface of the slag samples was polished using 600-, 1200-, and 2400-grid abrasive papers and finished using a 1-μm diamond slurry.

Table I. Basicity and f-CaO content (in mass%) of the industrial BOF and EAF slag samples used in this study.

Slag batch name	Type	Basicity	f-CaO*
Slag A	BOF	3.41	3.33
Slag B	BOF	3.27	2.99
Slag C	EAF (oxidizing)	2.15	0.49

*The f-CaO content was determined applying the ethylene glycol extraction method using ICP-AES.

The CL images and spectra of the slag samples were obtained using a custom scanning electron microscope CL (SEM-CL) system. Details regarding the SEM and acquisition of the CL images and spectra have been reported in our previous papers.[19,21-32] Briefly, the CL images were captured through a quartz viewport attached to a SEM (Mighty-8DXL, TECHNEX, Tokyo, Japan) *via* a digital mirrorless camera (α7RII, Sony Corp., Tokyo, Japan) equipped with a zoom lens (LZH-10A-05T, Seimitu Wave Inc., Kyoto, Japan). The detectable wavelength range of the camera was from 420 to 680 nm. The CL spectra of the slag samples were obtained using a spectrometer (QE65Pro, Ocean Optics Inc., Largo, Florida, USA). The light emitted from the slag samples was collimated using an off-axis parabolic mirror with a 0.5-mm hole at the center. Then, the collimated light was collected using a plano-convex lens attached to the tip of an optical fiber. The acceleration voltage of the SEM was set to 17 kV because we cannot change the voltage owing to the use of a permanent magnet for the condenser lens. We also conducted surface observations and elemental analyses of the slag samples using a SEM (TM3030 Plus, Hitachi High-Technologies Co., Tokyo, Japan) equipped with a silicon drift energy dispersive X-ray (EDX) detector (Quantax70, Bruker Corp., Billerica, Massachusetts, USA).

The XEOL image of the slag samples was captured using a custom setup comprising an X-ray tube with a rhodium target (TUB00050-RH2, Moxtek Inc., Orem, Utah, U.S.A.), and a digital mirrorless camera equipped with the same zoom lens used to obtain the CL images. The X-ray tube was operated at 30 kV and 200 μA. The details of the setup have been reported previously.[23,26,31,33]

3. RESULTS AND DISCUSSION

A. Determination of area fraction of f-CaO in BOF slag

Previous studies have reported that CaO reveals a CL peak at around 600 nm and orange luminescence in its CL images owing to Mn^{2+} that dissolved into CaO.[19,34] The CL peak and orange luminescence can be detected when the concentration of Mn in CaO is more than a few ppm.[35] In the present study, we attempted to determine the area fraction of f-CaO in industrial steelmaking slag from illuminated areas in CL images originating from f-CaO. Slag A contained mineral phases of β-belite (β-$2CaO{\cdot}SiO_2$), wüstite (FeO dissolving MgO and MnO), brownmillerite ($Ca_2(Al,Fe)_2O_5$), and f-CaO, which were confirmed *via* XRD, as presented in Fig. 1. The XRD peaks of CaO (37.84° and 54.54°) were shifted to higher angles than the reported peak positions of CaO owing to the dissolution of FeO and MnO into CaO. Figure 2(a) shows the SEM image of slag A; the corresponding EDX elemental mappings of Mg, Al, Si, P, Ca, Mn, and Fe are shown in Figs. 2(c), (d), (e), (f), (g), (h), and (i), respectively. Areas with high intensity of Ca Kα lines (Fig. 2(g)), such as areas 1 and 2 in Fig. 2(a), corresponded to f-CaO because their compositions (shown in Table II) were close to that of f-CaO dissolving FeO and MnO in previous reports.[36-38] Although we previously reported that f-CaO in steelmaking slag samples synthesized from reagents emits orange luminescence in CL images,[19] in this study, the areas that comprised f-CaO did not emit luminescence in slag A, as shown in Fig. 2(b). When slag A was heated at 600 °C, i.e., above the dehydration temperature of $Ca(OH)_2$ (approximately 450 °C[39]), for 10 min in air, the corresponding areas of f-CaO did not emit luminescence, as shown in supplementary Fig. S-1 (refer to electronic supplementary material). This indicated that a $Ca(OH)_2$ layer did not form on f-CaO in slag A. Moreover, the formation of $CaCO_3$ on f-CaO was also unconfirmed from the CL image of slag A (Fig. 2(b)) because $CaCO_3$ normally emits intense orange luminescence attributed to a CL peak at 620 nm.[19,34] However, blue-violet luminescence with low intensities was detected (Fig. 2(b)). All illuminated areas, such as areas 3 and 4 in Fig. 2(a), were confirmed to be $2CaO{\cdot}SiO_2$ *via* EDX point analysis (Table II). Figure 2(f) shows that the illuminated areas contained phosphorous, revealing that the areas comprised $2CaO{\cdot}SiO_2$ because phosphorous dissolves into $2CaO{\cdot}SiO_2$ as a $2CaO{\cdot}SiO_2$–$3CaO{\cdot}P_2O_5$ solid solution in BOF slag.[40-42] The CL spectrum of the $2CaO{\cdot}SiO_2$ (area 3) is shown in Fig. 3(a), wherein peaks were detected at 460 and 545 nm. The peak wavelengths were shorter than those of the $2CaO{\cdot}SiO_2$ we previously reported on (at 590 and 720 nm)[27] because the dissolution of phosphorous into the $2CaO{\cdot}SiO_2$ resulted in a shift of the peak positions to shorter wavelengths in the previous study.[43] We could speculate from Table II that the different luminescence colors of the $2CaO{\cdot}SiO_2$ between areas 3 and 4 may have been caused by the different phosphorous concentrations in the $2CaO{\cdot}SiO_2$. Areas with high intensity of Fe Kα lines (Fig. 2(i)), such as areas 5 and 6, and high intensity of Al Kα lines (Fig. 2(d)), such as area 7, were confirmed to be wüstite and $Ca_2(Al,Fe)_2O_5$, respectively, *via* EDX point analysis. No CL colors were detected in the areas comprising wüstite or $Ca_2(Al,Fe)_2O_5$.

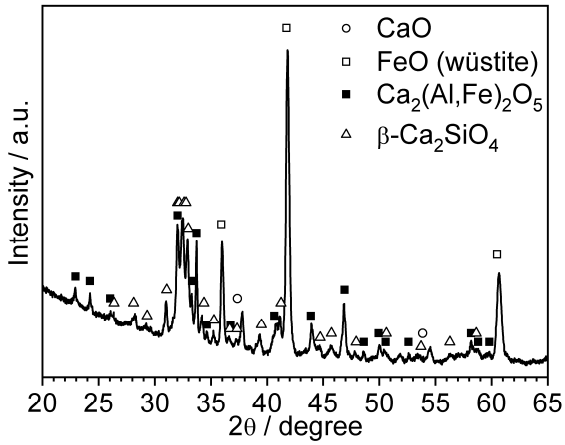

Fig. 1–XRD pattern of slag A.

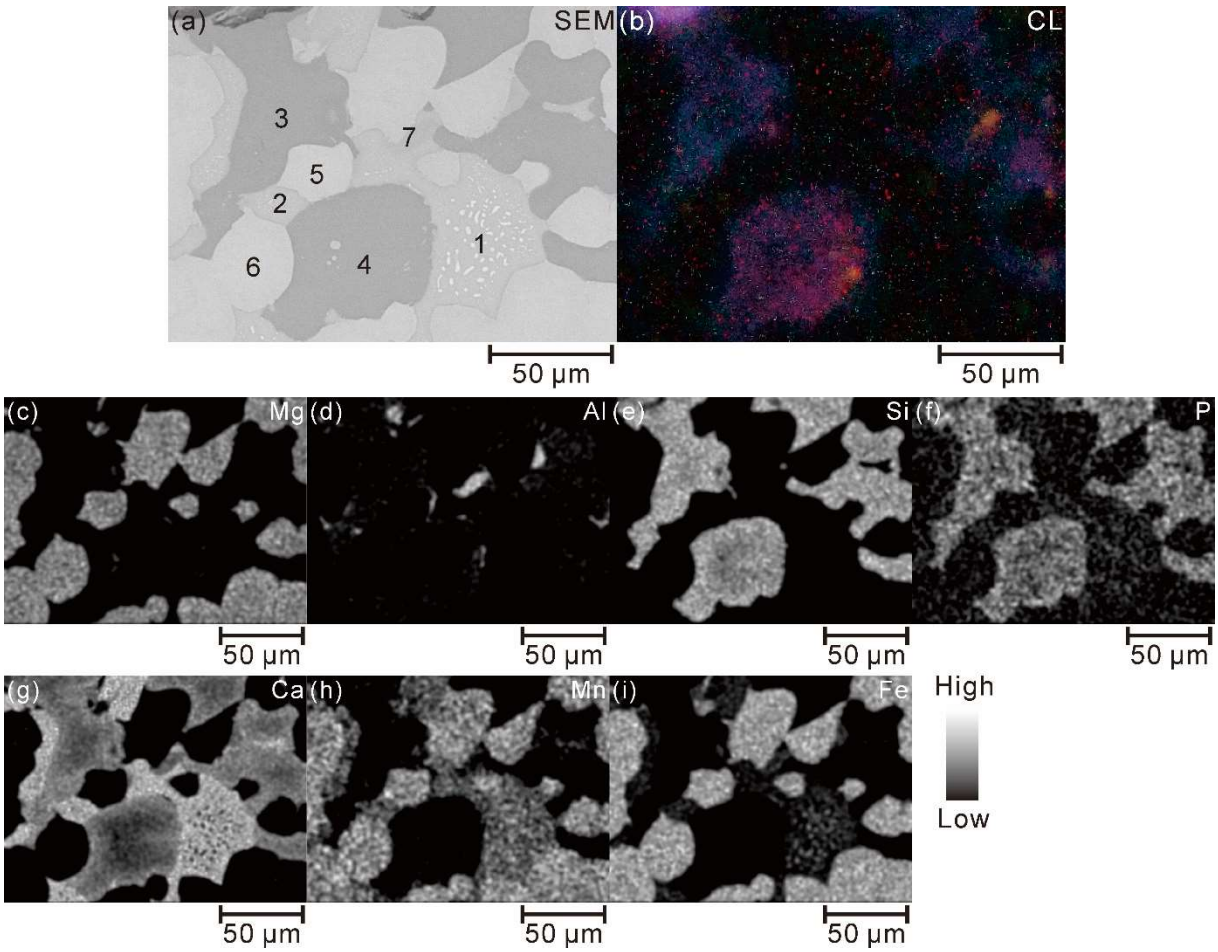

Fig. 2–(a) SEM (backscattered electron) image, (b) CL image, and EDX elemental mappings of (c) Mg, (d) Al, (e) Si, (f) P, (g) Ca, (h) Mn, and (i) Fe for slag A. The exposure time of the CL image was 100 s. (color)

Table II. Chemical compositions (in mol%) of areas 1 to 15 in Figs. 2(a), 3(a), 6(a), 7(a), 8(a), and 9 measured *via* EDX and their phases determined by EDX and XRD.

Area	Mg	Al	Si	P	Ca	Mn	Fe	Phases determined by EDX and XRD
1	4	<1	<1	<1	76	7	13	f-CaO
2	2	<1	<1	<1	79	7	12	f-CaO
3	1	1	25	3	68	<1	1	$2CaO{\cdot}SiO_2$
4	1	1	26	5	64	1	2	$2CaO{\cdot}SiO_2$
5	32	<1	<1	<1	4	12	52	Wüstite (FeO-MgO-MnO)
6	33	<1	<1	<1	4	11	51	Wüstite (FeO-MgO-MnO)
7	1	27	1	<1	53	1	16	$Ca_2(Al,Fe)_2O_5$
8	3	1	<1	<1	73	7	15	f-CaO
9	<1	1	26	2	70	<1	1	$2CaO{\cdot}SiO_2$*
11	2	33	22	1	40	<1	2	$2CaO{\cdot}Al_2O_3{\cdot}SiO_2$*
13	1	1	31	2	64	<1	1	$2CaO{\cdot}SiO_2$*
15	2	<1	<1	<1	80	3	15	f-CaO
16	3	<1	<1	<1	79	3	15	f-CaO

*These phases were determined by EDX alone.

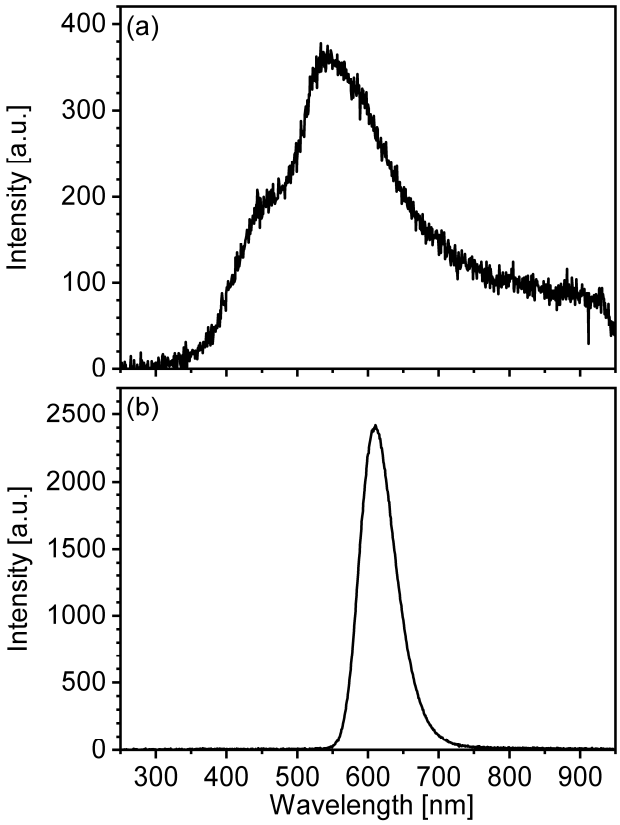

Fig. 3–CL spectra of (a) near area 4 (Fig. 2(a)) and (b) near area 8 (Fig. 4(a)). The acquisition times of the CL spectra for (a) and (b) were 100 and 10 s, respectively.

No clear luminescence from f-CaO was observed in the as-received industrial steelmaking slag samples. A previous study reported that luminescence from MgO, whose crystal structure is the same as that of CaO, is enhanced by heating and that the effect of the enhancement is promoted by increasing the heating temperature.[44] In preliminary experiments of our previous study,[19] we also experienced that CL intensity of f-CaO in steelmaking slag samples synthesized from reagents quenched from 1500 °C was higher than that quenched from 1300 °C, which might be related to the higher defect concentration in f-CaO at 1500 °C compared to that at 1300 °C. Based on these reports, when we placed slag A in a box furnace that had been already heated at 1000 °C in air, hold the slag for 3 min in the furnace, and then quenched to room temperature by taking the slag from the furnace and argon gas blowing on the slag, intense orange luminescence was observed in the CL image, as shown in Fig. 4(a). We selected the heat-treatment temperature of 1000 °C in the following reasons: (i) intense orange luminescence was not detected from f-CaO when the heat-treatment temperature was below 1000 °C and (ii) to prevent reactions among mineral phases in the slag during the heat-treatment. Most areas that emitted orange luminescence corresponded to f-CaO, which exhibited high intensity of Ca Kα lines in Fig 4(g). The illuminated area showed a CL peak at 600 nm (Fig. 3(b)), which agreed well with previously reported CL spectra of CaO and originated from Mn^{2+} substituting octahedrally coordinated calcium (II) ions (Ca^{2+}).[19,34] Orange luminescence was also observed along the grain-boundaries of wüstite, e.g., from area A to E in Fig. 4(a), due to f-CaO. Previous studies have reported that f-CaO precipitates along the grain-boundaries of wüstite in BOF slag.[37,45] Here, it was inferred that the amount of f-CaO precipitated along the grain-boundaries of the wüstite may have been small, since the grain-boundaries of the wüstite did not exhibit high intensity of Ca Kα lines (Figs. 2(g) and 4(g)). This could cause an overestimation of f-CaO amount. Luminescence related to $2CaO{\cdot}SiO_2$, which exhibited blue-violet luminescence before slag A was heated at 1000 °C, was not detected in the CL image in Fig. 4(a) because the CL intensities of f-CaO were over 50 times higher than those of the $2CaO{\cdot}SiO_2$ (Fig. 3). A comparison of Figs. 2 and 4 revealed that the microstructure of slag A remained unchanged by the heat-treatment because its elemental distributions were unchanged, indicating that the amount of f-CaO did not change because slag A did not include $Ca(OH)_2$. The reason why the f-CaO in slag A became excited enough to yield intense orange luminescence upon the heat-treatment was unclear. However, concerning the SEM-EDX analysis, there was no large difference in the concentrations of Mn in

f-CaO (the origin of the orange luminescence) before and after the heat-treatment, as shown in Table II (areas 1 and 8). Future work will be conducted to reveal the reason behind the f-CaO emission *via* an atomic scale analysis, such as transmission electron microscopy.

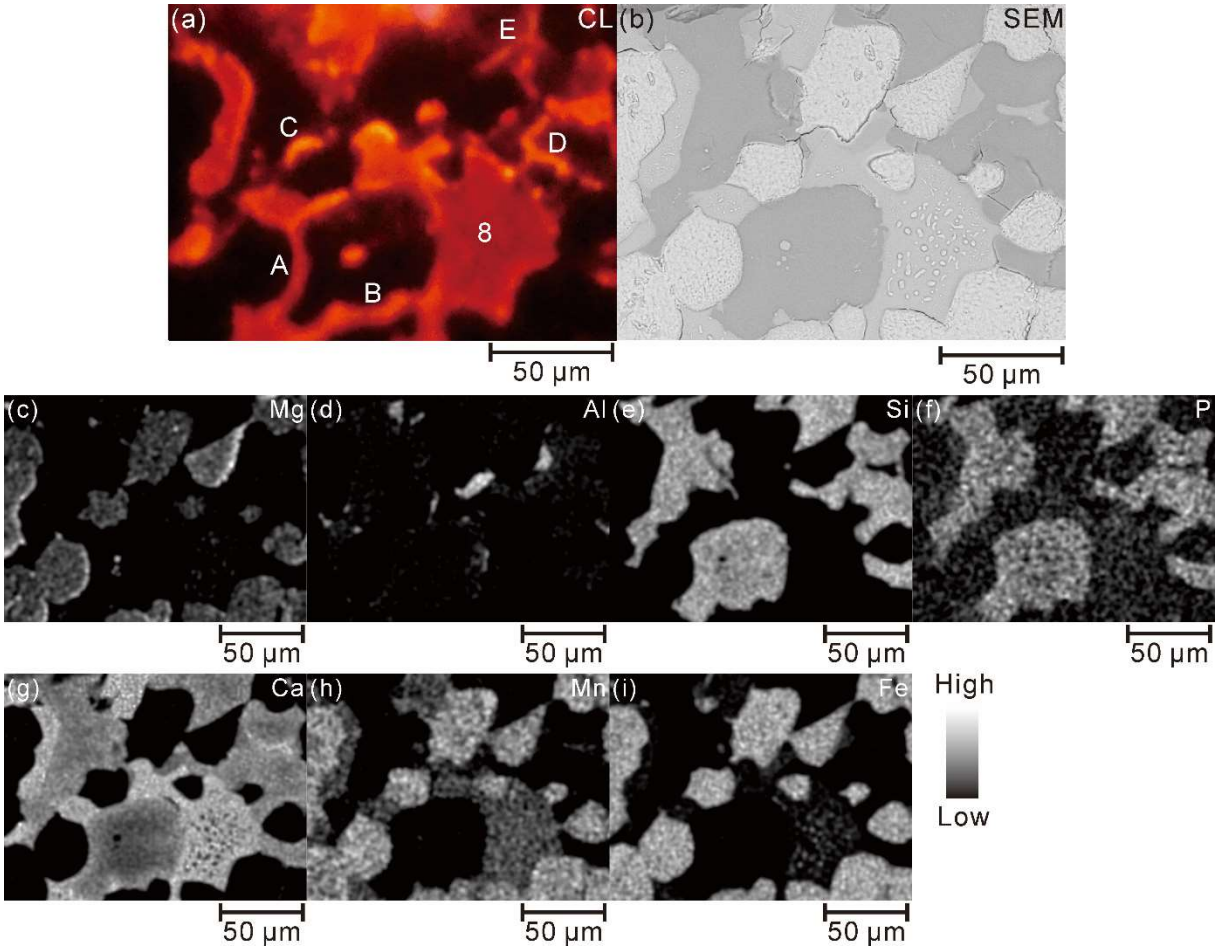

Fig. 4–(a) CL image, (b) SEM (backscattered electron) image, and EDX elemental mappings of (c) Mg, (d) Al, (e) Si, (f) P, (g) Ca, (h) Mn, and (i) Fe for slag A that was heated at 1000 °C for 3 min in air and quenched to room temperature. The area in this figure is the same as that in Fig. 2. The exposure time of the CL image was 10 s. (color)

We determined the area fraction of f-CaO in slag A from a fraction of the areas that emitted orange luminescence in the CL images of slag A that was heated at 1000 °C for 3 min in air and quenched to room temperature. We assumed that $Ca(OH)_2$ was not contained in slag A because none of the supplied slag samples had been aged and diffraction peaks related to $Ca(OH)_2$ were not detected *via* XRD (Fig. 1). In addition, we used slag samples that minimally contained $Ca(OH)_2$ for the measurements by cutting and polishing their surfaces. Five specimens in the batch of slag A were used for the measurements, and CL images were captured in at least five areas of each specimen. A typical CL image of slag A is shown in Fig. 5(a). The average fraction of areas that emitted orange luminescence in slag A was evaluated as 9.8% (Table III). We considered that the fraction of the evaluated areas were unaffected by the thickness of f-CaO because the detection depth of the CL analysis was a few micrometers at the accelerating voltage of 17 keV.[46] The f-CaO in slag B also emitted intense orange luminescence when the sample was heated at 1000 °C for 3 min and quenched, as shown in Fig. 5(b). The average fraction of areas that emitted orange luminescence in slag B was evaluated as 7.1% (Table III) by the same method as slag A. Note that the orange illuminated areas of f-CaO that appeared the along grain-boundaries of wüstite were overestimated.

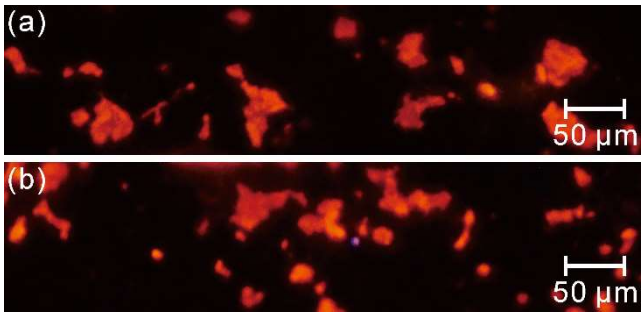

Fig. 5–Typical CL images of (a) slag A and (b) slag B that were heated at 1000 C for 3 min in air and quenched. The exposure times of the CL images of (a) and (b) were 2 and 3.2 s, respectively. (color)

Table III. Fraction of illuminated areas related to f-CaO and f-CaO content measured applying the ethylene glycol extraction method in slags A, B, and C.

	Fraction of illuminated areas related to f-CaO (%)	f-CaO content measured by ethylene glycol extraction method (mass%)
Slag A	9.8 ± 2.7	3.33
Slag B	7.1 ± 2.3	2.99
Slag C	0.9 ± 0.3	0.49

Our results provide a novel method to estimate approximate area fraction of f-CaO in industrial BOF slag by analyzing CL images more rapidly. However, to obtain more accurate f-CaO content measures in industrial BOF slag from CL images, it is crucial to investigate in detail the relationship between the contents and orange illuminated areas of f-CaO precipitating along the grain-boundaries of wüstite.

B. Determination of area fraction of f-CaO in EAF slag

We investigated the CL images and spectra of slag C to measure the area fraction of f-CaO in the industrial EAF slag sample. Orange and blue-violet luminescence were observed in a CL image of slag C after it had been heated at 1000 °C for 3 min in air and quenched, as shown in Fig. 6(a). These luminescent colors were similar to those observed in the BOF slag samples, which exhibited orange luminescence related to f-CaO and blue-violet luminescence related to $2CaO{\cdot}SiO_2$. The areas that emitted blue-violet luminescence, such as area 9 in Fig. 6(a), were confirmed to be $2CaO{\cdot}SiO_2$ *via* EDX analysis (Table II). The CL spectrum of area 9 agreed with that of area 4 in Fig. 2(a), as shown in Fig. 6(d), which indicated that the blue-violet illuminated areas here also comprised $2CaO{\cdot}SiO_2$. The areas that emitted orange luminescence did not correspond to the high intensity of Ca Kα line as shown in Fig. 6(c). However, the CL spectrum near the orange illuminated areas showed a peak at 600 nm, agreeing with that of f-CaO, and small peaks at 460 and 540 nm, agreeing with those of $2CaO{\cdot}SiO_2$ (area 9) (Fig. 6(d)). This indicated that f-CaO existed in the orange illuminated areas. We also detected red luminescence (e.g., area 11) and yellow luminescence (e.g., area 12) in another CL image of slag C, as shown in Fig. 7(a). The areas emitting this red luminescence were confirmed to be $2CaO{\cdot}Al_2O_3{\cdot}SiO_2$ *via* EDX analysis (Table II) and a reported pseudo-ternary phase diagram of Al_2O_3-CaO-SiO_2 system.[47] Peaks at 410 and 615 nm were detected in the CL spectrum of the $2CaO{\cdot}Al_2O_3{\cdot}SiO_2$ areas (Fig. 7(c)). However, we could not assign these peaks because no reports appeared to be available to index them. The CL spectrum near an area that emitted yellow luminescence (area 12) (Fig. 7(c)) consisted of the CL spectra of $2CaO{\cdot}Al_2O_3{\cdot}SiO_2$ and f-CaO, which revealed a peak at 600 nm, as the tail of that peak towards shorter wavelengths exhibited higher CL intensity than that of $2CaO{\cdot}Al_2O_3{\cdot}SiO_2$. Therefore, it was speculated that f-CaO also existed in the areas emitting yellow luminescence. Additionally, in a different area of slag C, blue-violet luminescence (e.g., area 13) and pale red luminescence (e.g., area 14) were detected in the CL image, as shown in Fig. 8(a). The CL spectrum of the areas emitting blue-violet luminescence (Fig. 8(c)) was consistent with that of the $2CaO{\cdot}SiO_2$ shown in Figs. 3(a) and 6(d) and confirmed to be $2CaO{\cdot}SiO_2$ *via* EDX analysis (Table II). The CL spectrum of the areas emitting pale red luminescence was almost the same as that of $2CaO{\cdot}SiO_2$, except for a peak at 755 nm, as shown in Fig. 8(c). However, the peak at 755 nm was in good agreement with a CL peak of free magnesia (f-MgO).[27,30,48-50] The detection of f-MgO was expected because industrial steelmaking slag includes a few mass% of f-MgO.[9,17,38,51] Therefore, f-MgO existed in the areas that emitted pale red luminescence,

whereas f-CaO did not. The CL colors and peaks of the mineral phases detected in the present study are summarized in Table IV.

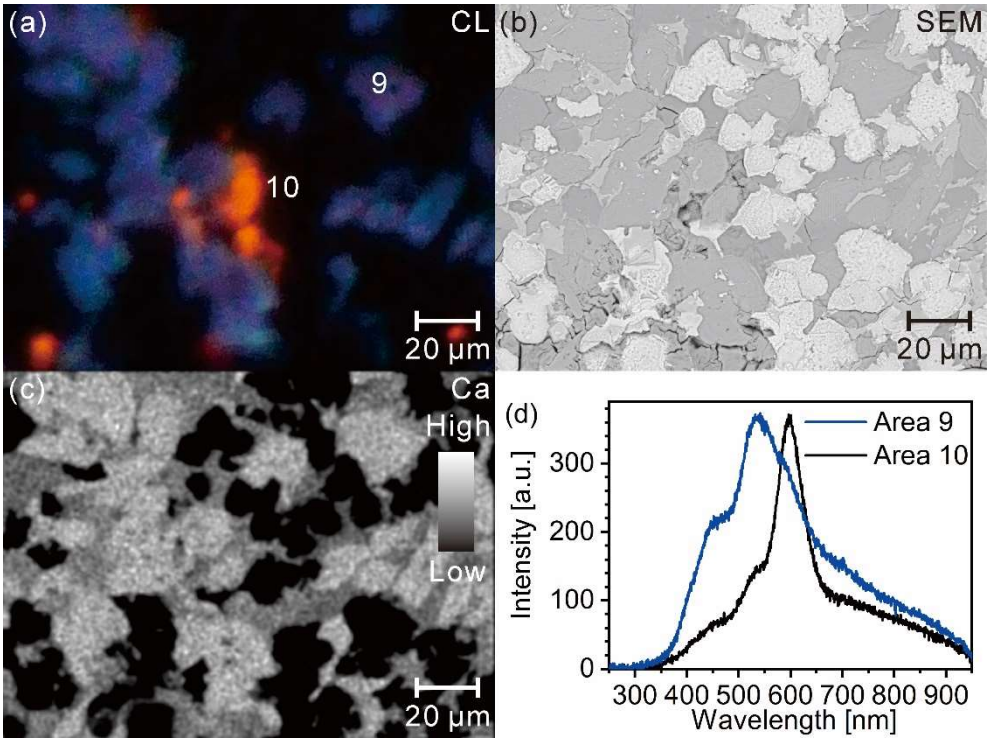

Fig. 6–(a) CL image, (b) SEM (backscattered electron) image, and (c) EDX elemental mapping of Ca for slag C that was heated at 1000 °C for 3 min in air and quenched. The exposure time of the CL image was 2 s. (d) CL spectra of areas 9 and 10 in (a). The measurement time of the CL spectra was 10 s. (color)

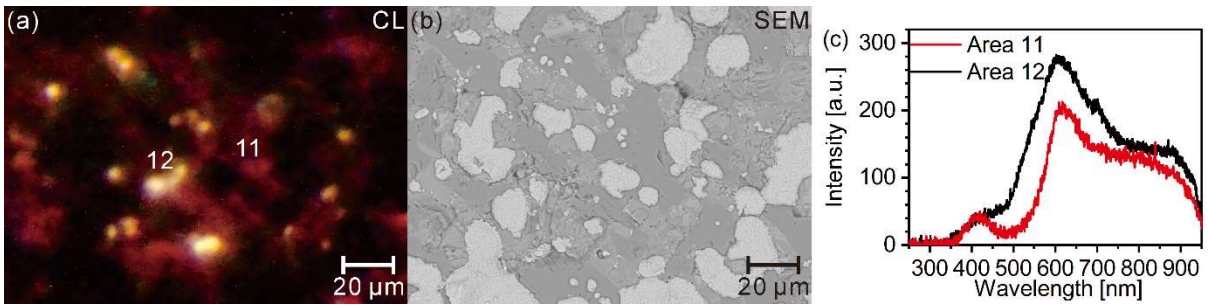

Fig. 7–(a) CL image, (b) SEM (backscattered electron) image of slag C that was heated at 1000 °C for 3 min in air and quenched. The exposure time of the CL image was 30 s. (C) CL spectra of areas 11 and 12 in (a). The measurement time of the CL spectra was 30 s. (color)

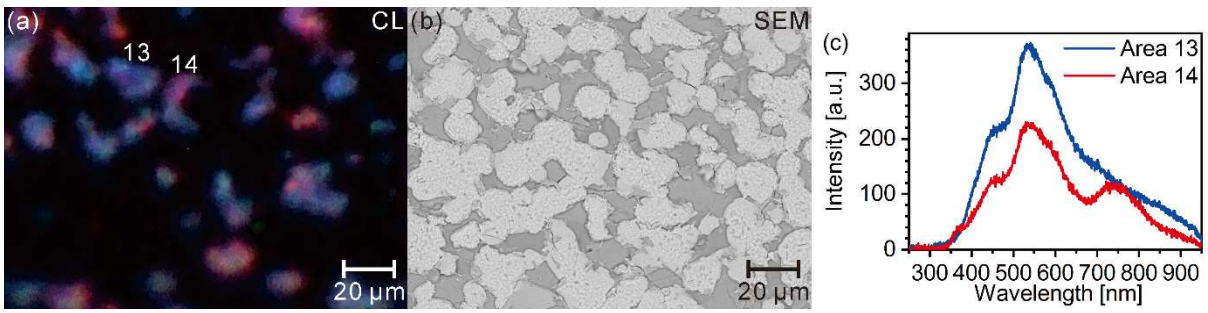

Fig. 8–(a) CL image, (b) SEM (backscattered electron) image of slag C that was heated at 1000 °C for 3 min in air and quenched. The exposure time of the CL image was 10 s. (C) CL spectra of area 13 and 14 in (a). The measurement time of the CL spectra was 10 s. (color)

Table IV. CL color and CL peak wavelength for mineral phases detected in the present study.

Color	Wavelength (nm)	Mineral phase
Orange	600	Free lime (f-CaO)
Blue-violet	460, 545	$2CaO{\cdot}SiO_2$
Red	410, 615	$2CaO{\cdot}Al_2O_3{\cdot}SiO_2$
Yellow	410, 600, 615	f-CaO and $2CaO{\cdot}Al_2O_3{\cdot}SiO_2$
Pale red	460, 545, 755	$2CaO{\cdot}SiO_2$ and free magnesia (f-MgO)
–*	–	wüstite
–	–	$Ca_2(Al,Fe)_2O_5$

* – means not detected.

We confirmed that the areas in slag C emitting orange and yellow luminescence included f-CaO by investigating the sample's CL images and spectra. Subsequently, the area fraction of f-CaO in slag C was determined from the fractions of these areas in the same way as the BOF slag samples. Five specimens in the batch of slag C were used for the measurements, and CL images were captured in at least six areas of each slag. Typical CL images of slag C are shown in supplementary Fig. S-2 (refer to electronic supplementary material). Both the fractions of the illuminated areas and f-CaO contents decreased in the order of slags A, B, and C (Table III). Thus, the area fractions of f-CaO in industrial BOF and EAF slag can be roughly obtained by evaluating a fraction of the illuminated areas in CL images originating from f-CaO.

C. *Determination of area fraction of f-CaO in steelmaking slag from XEOL image*

In this study, we established a method to determine the area fraction of f-CaO in industrial steelmaking (BOF and EAF) slag by capturing CL images. Acquiring XEOL images would enable on-site determination of the area fraction of f-CaO because the XEOL method can be performed in the air in contrast with the CL method's requirement for a vacuum condition. We captured an XEOL image of slag A after the specimen was heated at 1000 °C for 3 min and quenched to room temperature, as shown in Fig. 9(a). The areas that emitted orange luminescence were confirmed to be f-CaO *via* EDX analysis (Table II). The XEOL image was clear and bright enough to determine the area fraction of f-CaO in slag A, when the exposure time of the XEOL image was 30 s, i.e., approximately 15 times longer than that of CL image. This result indicated that XEOL images can be obtained for on-site analyses of the area fraction of f-CaO in industrial steelmaking slag.

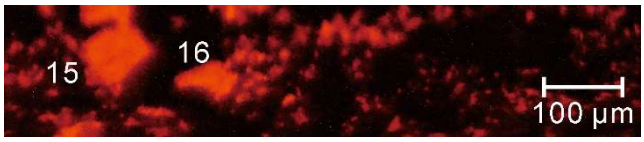

Fig. 9–XEOL image of slag A that was heated at 1000 °C for 3 min in air and quenched to room temperature. The exposure time of the XEOL image was 30 s. (color)

In the present study, we analyzed the industrial steelmaking slag whose $Ca(OH)_2$ and $CaCO_3$ contents were low. When the steelmaking slag contained $CaCO_3$, we could identify luminescence related to $CaCO_3$ by capturing CL images of the steelmaking slag prior to the heat-treatment at 1000 °C because $CaCO_3$ precipitated after the aging of steelmaking slag emits intense luminescence at CL peak of 620 nm, as demonstrated in our previous study.[19] However, the area fraction of f-CaO may be difficult to determine from the CL images of steelmaking slag that includes $Ca(OH)_2$ because luminescence intensity related to $Ca(OH)_2$ is low and the $Ca(OH)_2$ may be dehydrated to CaO by the heat-treatment at 1000 °C. However, speciation between f-CaO and $Ca(OH)_2$ is rarely conducted even by chemical analysis using the ethylene glycol extraction method. Future work should focus on distinguishing f-CaO from $Ca(OH)_2$ in CL images by investigating the CL spectrum and color of $Ca(OH)_2$, heat-treatment conditions required to obtain intense f-CaO emissions for industrial steelmaking slag (heating temperatures, holding times, etc.), and morphologies of $Ca(OH)_2$ precipitated from steelmaking slag. Nevertheless, the method we presented here is promising for the determination of f-CaO in steelmaking slag because of its simplicity and rapidness compared with the ethylene glycol extraction method, which is most commonly employed.

4. CONCLUSIONS

We have proposed a simple practical method to roughly determine the area fraction of f-CaO in industrial steelmaking (BOF and EAF) slag from a fraction of illuminated areas originating from f-CaO in CL and XEOL images. The f-CaO in the slag emitted intense luminescence at a peak of 600 nm in the images when heated at 1000 °C in air and then quenched to room temperature. This heat-treatment was essential to obtain the luminescence related to the f-CaO in slag by-produced in the practical steelmaking process. The area fractions of the f-CaO evaluated from the CL images roughly followed the f-CaO contents determined by chemical analysis applying the ethylene glycol extraction method; the order of the f-CaO contents in the three steelmaking slag samples studied was consistent with that of the area fractions of the f-CaO in the CL images. Thus, acquiring CL and XEOL images are a simple yet powerful method to appropriately determine the area fraction of f-CaO in industrial steelmaking slag. In particular, the acquisition of XEOL images is promising for practical analyses because it is applicable for on-site analyses. To improve the accuracy of f-CaO content determined *via* this method, a relationship between the contents and illuminated areas of f-CaO precipitated along the grain-boundary of wüstite must be further investigated. Future work will apply this method in determining f-CaO content in industrial steelmaking slag including $Ca(OH)_2$. Thus, for the practical application of this method, precise evaluation of f-CaO precipitated along the grain-boundary of wüstite and distinguishing between f-CaO and $Ca(OH)_2$ are required.

Acknowledgments

This study was supported by Steel Foundation for Environmental Protection Technology. We would like to thank Nippon Steel Corp. and JFE Steel Corp for the supplies of steelmaking slag samples and for the determination of their f-CaO contents.

References

1. S.-Y. Pan, R. Adhikari, Y.-H. Chen, P. Li and P.-C. Chiang: *J. Clean Prod.* 2016, vol. 137, pp. 617-631.
2. İ. Yüksel: *Environ. Dev. Sustain.* 2016, vol. 19, pp. 369-384.
3. Y. Jiang, T.-C. Ling, C. Shi and S.-Y. Pan: *Resour. Conserv. Recycl.* 2018, vol. 136, pp. 187-197.
4. A. Panis: *Bull. Eng. Geol. Environ.* 1984, vol. 30, pp. 449-451.
5. G. Wang, Y. Wang and Z. Gao: *J. Hazard. Mater.* 2010, vol. 184, pp. 555-560.
6. C. Kambole, P. Paige-Green, W.K. Kupolati, J.M. Ndambuki and A.O. Adeboje: *Constr. Build. Mater.* 2017, vol. 148, pp. 618-631.
7. S. Chatterji: *Cem. Concr. Res.* 1995, vol. 25, pp. 51-56.
8. L.F. Amaral, I.R. Oliveira, P. Bonadia, R. Salomão and V.C. Pandolfelli: *Ceram. Int.* 2011, vol. 37, pp. 1537-1542.
9. L.M. Juckes: *Trans. Inst. Min. Metall., Sect. C* 2003, vol. 112, pp. 177-197.
10. D.R. MacPherson and L.R. Forbrich: *Ind. Eng. Chem. Anal. Ed.* 1937, vol. 9, pp. 451-453.
11. M.P. Javellana and I. Jawed: *Cem. Concr. Res.* 1982, vol. 12, pp. 399-403.
12. M. Bartl and D. Pekárek: *Analyst* 1972, vol. 97, pp. 848-853.
13. J. Vaverka and K. Sakurai: *ISIJ Int.* 2014, vol. 54, pp. 1334-1337.
14. K. Tanaka, M. Narita and K. Watanabe: *Tetsu To Hagane-J. Iron Steel Inst. Jpn.* 2014, vol. 100, pp. 1386-1390.
15. S. Michikawa, A. Ono and H. Eba: *Tetsu To Hagane-J. Iron Steel Inst. Jpn.* 2016, vol. 102, pp. 623-629.
16. Y. Fujioka, M. Aimoto and M. Nishifuji: *CAMP-ISIJ* 2009, vol. 22, p. 683.
17. M. Kato, K. Tsukagoshi, M. Aimoto, S. Saito and M. Shibukawa: *ISIJ Int.* 2018, vol. 58, pp. 1834-1839.
18. M. Kato, T. Hari, S. Saito and M. Shibukawa: *Tetsu To Hagane-J. Iron Steel Inst. Jpn.* 2014, vol. 100, pp. 340-345.
19. H. Tsuneda, S. Imashuku and K. Wagatsuma: *Tetsu To Hagane-J. Iron Steel Inst. Jpn.* 2019, vol. 105, pp. 30-37.
20. Chemical composition of iron and steel slag (Nippon Slag Association Web, 2020), http://www.slg.jp/e/slag/character.html Accessed 15 June 2020.
21. S. Imashuku, K. Ono and K. Wagatsuma: *X-Ray Spectrom.* 2017, vol. 46, pp. 131-135.
22. S. Imashuku, K. Ono, R. Shishido, S. Suzuki and K. Wagatsuma: *Mater. Charact.* 2017, vol. 131, pp. 210-216.
23. S. Imashuku, K. Ono and K. Wagatsuma: *Microsc. Microanal.* 2017, vol. 23, pp. 1143-1149.
24. S. Imashuku and K. Wagatsuma: *Metall. Mater. Trans. B* 2018, vol. 49B, pp. 2868-2874.
25. S. Imashuku and K. Wagatsuma: *Surf. Interface Anal.* 2019, vol. 51, pp. 31-34.

26. S. Imashuku and K. Wagatsuma: *X-Ray Spectrom.* 2019, vol. 48, pp. 522-526.
27. S. Imashuku, H. Tsuneda and K. Wagatsuma: *Metall. Mater. Trans. B* 2020, vol. 51B, pp. 28-34.
28. S. Imashuku and K. Wagatsuma: *Metall. Mater. Trans. B* 2020, vol. 51B, pp. 79-84.
29. S. Imashuku and K. Wagatsuma: *Oxid. Met.* 2019, vol. 93, pp. 175-182.
30. S. Imashuku, H. Tsuneda and K. Wagatsuma: *Spectrochim. Acta, Part A* 2020, vol. 229, p. 117952.
31. S. Imashuku and K. Wagatsuma: *Corros. Sci.* 2019, vol. 154, pp. 226-230.
32. S. Imashuku and K. Wagatsuma: *Miner. Eng.* 2020, vol. 151, p. 106317.
33. S. Imashuku and K. Wagatsuma: *Oxid. Met.* 2020, in press.
34. L. Feng, Z. Hao, X. Zhang, L. Zhang, G. Pan, Y. Luo, L. Zhang, H. Zhao and J. Zhang: *Dalton Trans.* 2016, vol. 45, pp. 1539-45.
35. D. Habermann, R.D. Neuser and D.K. Richter: In *Cathodoluminscence in Geosciences*, ed. M. Pagel, Barbin V., Blanc P. and Ohnenstetter D. Springer: Berlin, 2000, pp 331-358.
36. H. Suito, T. Yokomaku, Y. Hayashida and Y. Takahashi: *Tetsu To Hagane-J. Iron Steel Inst. Jpn.* 1977, vol. 63, pp. 2316-2325.
37. A. Niida, K. Okohira, A. Tanaka and T. Kai: *Tetsu To Hagane-J. Iron Steel Inst. Jpn.* 1983, vol. 69, pp. 42-50.
38. M. Gautier, J. Poirier, F. Bodénan, G. Franceschini and E. Véron: *Int. J. Miner. Process.* 2013, vol. 123, pp. 94-101.
39. J. Zelić, D. Rušić and R. Krstulović: *J. Therm. Anal. Calorim.* 2002, vol. 67, pp. 613-622.
40. W. Fix, H. Heymann and R. Heinke: *J. Am. Ceram. Soc.* 1969, vol. 52, pp. 346-347.
41. H. Suito, Y. Hayashida and Y. Takahashi: *Tetsu To Hagane-J. Iron Steel Inst. Jpn.* 1977, vol. 63, pp. 1252-1259.
42. R. Inoue and H. Suito: *ISIJ Int.* 2006, vol. 46, pp. 174-179.
43. Z. Mao, Z. Lu, J. Chen, B.D. Fahlman and D. Wang: *Journal of Materials Chemistry C* 2015, vol. 3, pp. 9454-9460.
44. J. Götze: In *Cathodoluminscence in Geosciences*, ed. M. Pagel, Barbin V., Blanc P. and Ohnenstetter D. Springer: Berlin, 2000.
45. R. Inoue and H. Suito: *ISIJ Int.* 1995, vol. 35, pp. 272-279.
46. B.G. Yacobi and D.B. Holt: In *Cathodoluminescence Microscopy of Inorganic Solids*, Plenum Press: New York, 1990, pp 151-155.
47. V.D. Eisenhüttenleute: *Slag Atlas*, 2nd ed. Verlag Stahleisen, Düsseldorf, 1995.
48. T.A. Vu, J. Götze, K. Burkhardt, J. Ulbricht and D. Habermann: *Int. Ceram.* 1998, vol. 47, pp. 164-167.
49. M. Karakus, M.D. Crites and M.E. Schlesinger: *J. Microsc.* 2000, vol. 200, pp. 50-58.
50. C.M. MacRae and N.C. Wilson: *Microsc. Microanal.* 2008, vol. 14, pp. 184-204.
51. K. Kanehashi and M. Aimoto: *Tetsu To Hagane-J. Iron Steel Inst. Jpn.* 2013, vol. 99, pp. 543-551.

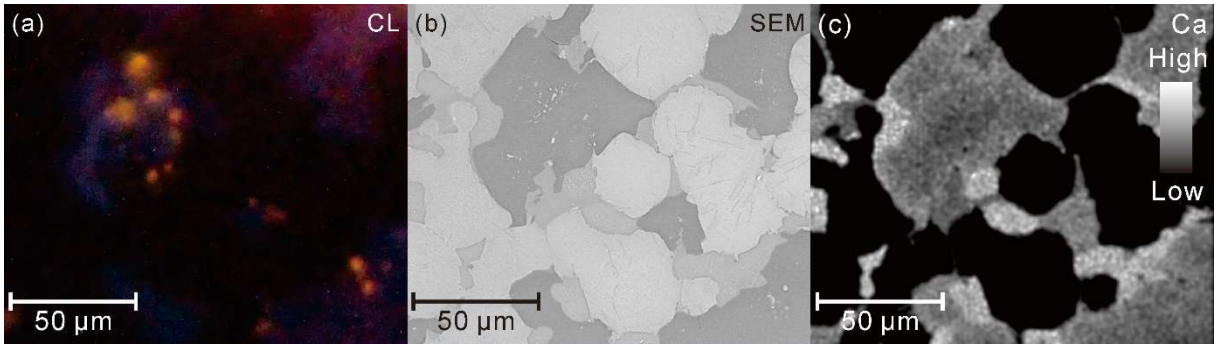

Fig. S-1 CL, SEM images, and EDX elemental mappings of Ca of slag A that was heated at 600 °C for 10 min and quenched to room temperature. Free lime was confirmed in areas with high intensities of Ca Kα in (c) by EDX point analysis.

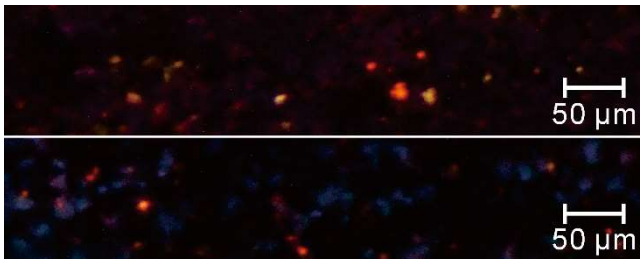

Fig. S-2 Typical CL images of slag C that was heated at 600 °C for 10 min and quenched to room temperature. The exposure time for the CL images were 10 s.